

## Response to Anonymous Referee #2

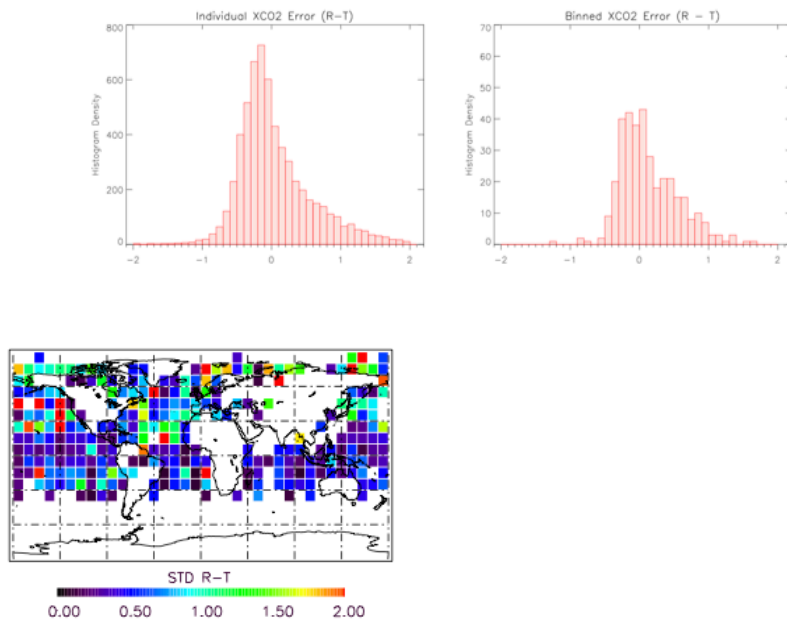
We thank referee #2 for a careful review and insightful questions and comments. We address his/her comments sequentially below.

Many comments by both reviewers can only be addressed appropriately with revisions to the text and/or figures in the manuscript. Therefore we have prepared a revised manuscript and will include it by reference below.

### Comment #1:

It was never our intention to quantitatively assess the error analysis based on the difference between the 'true' and retrieved results (hereafter R-T). There are 2 reasons for this: first, the main function of such a comparison would be to check the agreement of mathematics and programming of the orbit simulator, retrieval codes, and the error analysis calculations, rather than our understanding of the atmosphere. Second, the R-T results are not directly comparable to the error analysis, in that no forward model errors are present in R-T, because the same spectroscopic and instrument parameters are used in both the orbit simulator and the L2 retrieval code. Further, the ensemble variability of the state vector elements in the real atmosphere must be estimated in the error analysis; the data set of model soundings is too small to reproduce this ensemble variability accurately, and no attempt has been made to do so. Thus we don't believe such a comparison is an important element in presenting these results; nevertheless it is a useful internal 'sanity' check on our calculations, and we have made such comparisons from time to time. We include example figures below, although we do not include them in the paper.

### Retrieved – True Values (ppm), June, Ocean



Standard deviation of the R-T values for ocean observations, June. This figure may be approximately compared to the left hand panel in the second row of Fig. 5

Comment #2:

The earlier study (Connor et al, 2008) was primarily concerned with the 'objective, design, and implementation of the OCO inverse method'. It also described the off-line error analysis formulation and code which has been used in the present study, and gave examples, presenting an 'illustration by prospective application to case studies'

There are many quantitative differences between the error estimates of the 2 studies, based on the difference between OCO and OCO-2, and the development of the sophistication of the algorithm (for one thing, its treatment of aerosols) over nearly 10 years (Connor et al 2008 was submitted for publication in 2006). Further, the current paper uses a much more sophisticated treatment of the inputs to the error estimates, including the aerosol ensemble variability, spectroscopic uncertainties, and instrument calibration uncertainties. In hindsight, it is fair to say that the aerosol errors, particularly in the Southern Hemisphere, were underestimated in Connor et al (2008), by a few tenths of a ppm (compare Fig 7 of Connor et al (2008) to Fig. 4a of the current paper)

However we don't believe publishing a quantitative comparison of the 2 papers' error estimates would serve any useful purpose; we have applied the error analysis formulation of Connor et al, (2008), as referenced in the introduction to Sect 2 and 2.1, and believe that is the appropriate relationship between the two works.

Comment #3:

The determination of errors in XCO<sub>2</sub> gradients is key to scientific interpretation of the OCO-2 measurements, and the reviewer has been very perceptive to probe further into the nature of 'variable error' and the role of 'fixed error sources' in producing variable error. We will expand and clarify the discussion of these concepts in the paper as follows:

In the abstract we will add the sentence "Spectroscopy and calibration, although they are themselves fixed error sources, also produce important variable errors in XCO<sub>2</sub>." In section 5 we add "the remaining, variable error, caused by the fixed error sources, is of critical importance."

The reviewer asks whether the "variable error" is "really the difference between any two soundings or rather the difference between two spatiotemporally close soundings?" In section 2.3 we have added this discussion:

"By its nature, variable error has both random components and those which are systematic in the sense that they depend on conditions such as solar zenith angle, atmospheric temperature, pressure, and aerosol, and surface properties. In other words, the concept of variable error applies to the difference between any two soundings, but its magnitude will depend on the difference in conditions between them."

Spatiotemporally close soundings will on average have more similar sounding conditions, and thus less variable error, than more distant soundings.

Comment #4:

This is an important question which we considered carefully in assembling the list of spectroscopic parameters in Table 1, ultimately deciding that no parameters of interfering species need be included. We have now added a short paragraph in section 3.4 discussing this conclusion.

Comment #5:

The gain function, and thus the averaging kernels, are the properties of the retrieval as actually performed, i.e. they depend on the Jacobians at the retrieved state rather than the true state.

Also, the assumption behind use of linear analysis is that the forward model is (approximately) linear within the error bounds of the retrieval; given that is true, the difference between using the true and retrieved states to calculate the Jacobians will be insignificant.

Comment #6:

The correction of in-orbit degradation of the calibration has not been included.

Comment #7:

Fig 4c has been added to the revised manuscript, showing the MERRA AOD variability. The supplementary material has been explicitly referred to in the text after introducing Fig 4.

Comment #8:

The references in sections 1 and 2 have been expanded to include 4 additional papers addressing the GOSAT retrieval algorithm and earlier assessments of error sensitivity for OCO-2 and GOSAT.

## Quantification of Uncertainties in OCO-2 Measurements of XCO<sub>2</sub>: Simulations and Linear Error Analysis

5 Brian Connor<sup>1</sup>, Hartmut Bösch<sup>2,6</sup>, James McDuffie<sup>3</sup>, Tommy Taylor<sup>4</sup>, Dejian Fu<sup>3</sup>,  
Christian Frankenberg<sup>5</sup>, Chris O'Dell<sup>4</sup>, Vivienne H. Payne<sup>3</sup>, Michael Gunson<sup>3</sup>, Randy  
Pollock<sup>3</sup>, Jonathan Hobbs<sup>3</sup>, Fabiano Oyafuso<sup>3</sup>, and Yibo Jiang<sup>3</sup>

<sup>1</sup> BC Scientific Consulting, Stony Brook, NY, USA

10 <sup>2</sup> EOS Group, Department of Physics and Astronomy, University of Leicester,  
Leicester, UK

<sup>3</sup> Jet Propulsion Laboratory, California Institute of Technology, Pasadena, CA, USA

<sup>4</sup> Cooperative Institute for Research in the Atmosphere, Fort Collins, CO, USA

<sup>5</sup> California Institute of Technology, Pasadena, CA, USA

15 <sup>6</sup> National Centre for Earth Observation NCEO, University of Leicester, Leicester, UK

*Correspondence to:* Brian Connor (bc.scientific.consulting@gmail.com)

20 **Abstract.** We present an analysis of uncertainties in global measurements of the  
column averaged dry-air mole fraction of CO<sub>2</sub> ('XCO<sub>2</sub>') by the NASA Orbiting  
Carbon Observatory-2, ('OCO-2'). The analysis is based on our best estimates for  
uncertainties in the OCO-2 operational algorithm and its inputs, and uses simulated  
25 spectra calculated for the actual flight and sounding geometry, with measured  
atmospheric analyses. The simulations are calculated for land nadir and ocean glint  
observations. We include errors in measurement, smoothing, interference, and  
forward model parameters. All types of error are combined to estimate the uncertainty  
in XCO<sub>2</sub> from single soundings, before any attempt at bias correction has been made.  
From these results we also estimate the 'variable error' which differs between  
30 soundings, to infer the error in the difference of XCO<sub>2</sub> between any two soundings.  
The most important error sources are aerosol interference, spectroscopy, and  
instrument calibration. Aerosol is the largest source of variable error. Spectroscopy  
and calibration, although they are themselves fixed error sources, also produce  
important variable errors in XCO<sub>2</sub>. Net variable errors are usually < 1 ppm over ocean  
35 and ~0.5 – 2.0 ppm over land. The total error due to all sources is ~1.5 – 3.5 ppm over  
land, ~1.5 – 2.5 ppm over ocean.

40

## 1. Introduction

Brian Connor 22/9/2016 9:35 AM

Deleted: -

... [1]

The Orbiting Carbon Observatory-2 (OCO-2) was launched on July 2, 2014 and has been making global measurements of CO<sub>2</sub> and O<sub>2</sub> spectral bands in reflected sunlight since early September 2014. Spectra are recorded in two CO<sub>2</sub> bands at 1.61 μm and 2.06 μm ('WCO<sub>2</sub>' and 'SCO<sub>2</sub>', respectively), and the O<sub>2</sub> A-band at 0.76 μm with a resolving power between 17000 and 20000. These measurements are analyzed to provide estimates of the column-averaged dry-air mole fraction of CO<sub>2</sub>, known as XCO<sub>2</sub>. Details of the OCO-2 mission, measurement technique, and XCO<sub>2</sub> retrieval may be found in Crisp et al, (2008) and O'Dell et al, (2012). The instrument calibration is detailed in Rosenberg et al, (2016) and Lee et al, (2016). [An overview of the results to be expected from OCO-2 was given by Bösch et al \(2011\).](#) These measurements are motivated primarily by the need to infer regional carbon fluxes, and to constrain global models of the carbon cycle. Characterizing the uncertainties in XCO<sub>2</sub> as measured, and in how these uncertainties vary in space and time, is critical for this purpose. [Earlier studies of the error to be expected from such observations include Butz et al, \(2009\) and Jung et al, \(2016\).](#) The present study is part of the ongoing effort at uncertainty quantification for the OCO-2 mission.

In this paper we assess the uncertainty in a single XCO<sub>2</sub> sounding by 'bottom-up' analysis, using the best available estimates of errors in the algorithm and its inputs ('error sources'), computing the contribution of each error source to uncertainty in XCO<sub>2</sub>, and combining them to estimate net uncertainty. We further estimate the uncertainty in the difference of XCO<sub>2</sub> between any two soundings, by excluding the mean error produced by error sources which are constant in themselves. We compare XCO<sub>2</sub> uncertainties and their variability over land (nadir) and ocean (glint) for both June and December simulated data sets. Finally, we summarize the effect of all error sources globally, and identify those which are largest and most variable.

Our methodology is described in detail in Sections 2 and 3 below. In overview, simulations of OCO-2 spectra were run with the CSU orbit simulator (O'Brien et al., 2009), retrievals were performed with the operational Level-2 (L2) code, and a linear

Brian Connor 22/9/2016 9:35 AM

Formatted: Space After: 12 pt, Tabs: 0.39 cm, Left + 1.27 cm, Left

error analysis was performed using a dedicated off-line code. This study used simulations to allow full control of the calculations and their inputs. The use of simulations for this analysis should not significantly affect its overall conclusions or their applicability to OCO-2 operational measurements, since the simulations are calculated from ‘true states’ drawn from a realistic atmosphere.

Simulated spectra were calculated for 3 days in June and 3 in December. Only nadir spectra were calculated over land, and only glint spectra over ocean. Calculations were done for a single footprint (as opposed to 8 footprints for the flight data), with the sounding frequency set at 1 Hz (as compared to 3 Hz in operation). The resulting reduction in data volume (factor of 24) was done purely for convenience and should not affect conclusions from this study. After cloud screening using the Oxygen A-Band Preprocessor (ABP) (Taylor, et al, 2016), the operational L2 code was run on the simulations, and the results screened for convergence. A second screen was performed to minimize the occurrence of outliers, by restricting the accepted range of some sounding and retrieved parameters. More than 20 thousand soundings passed these screens, and those were run with the L2 code a second time, using an extended state vector including a set of interfering aerosols. The interfering aerosols are tightly constrained to very small values in this step, but are included to force the L2 code to calculate their Jacobians. The Jacobian matrix,  $K$ , for the extended state vector was saved for later analysis. (The Jacobian matrix contains the first order partial derivatives of the forward model with respect to the state vector elements, i.e.,  $K=dF(x)/dx$ ). In addition, Jacobians were evaluated for a range of forward model errors, and also saved.

Linear error analysis (Rodgers, 2000, Rodgers & Connor, 2003) was performed on the extended L2 output, using an off-line code developed for the purpose (Connor et al, 2008). We calculate actual uncertainties using estimates of true error in the measured spectrum, the variability of the atmospheric ensemble, and forward model errors. These calculations are intended to apply to a comparison of L2 results to the true atmospheric values, without applying a ‘bias correction’ (Wunch, et al, 2011) to the L2 results.

The paper is organized as follows. In Sect. 2 we briefly discuss the L2 retrieval algorithm and then present details of the error analysis methodology. This is followed by an enumeration and discussion of the error sources to be considered in Sect. 3. Sect. 4 contains the results of the linear error analysis. Sect. 5 is a discussion of the results, and Sect. 6 identifies needs for future research.

## 2. Background and Methodology

The OCO-2 level 2 full physics retrieval algorithm ('L2'), consists of a forward model and inverse method, described in full detail in JPL (2015). The forward model is a radiative transfer model of the atmosphere coupled to a model of the solar spectrum to calculate the monochromatic spectrum at the top of the atmosphere, which is then convolved with the response function as measured for the OCO-2 instrument. The inverse method is a maximum a posteriori likelihood method of a type which has been widely used in the community (Rodgers, 2000; Rodgers & Connor, 2003; Connor et al, 2008, O'Dell et al, 2012). [For comparison, the retrieval algorithm for the spectrally similar measurements by the GOSAT satellite is described in Yoshida et al \(2011\).](#) Uncertainty in the OCO-2 measurements of XCO<sub>2</sub> has been assessed using an off-line error analysis code developed for the purpose (Connor et al, 2008).

### 2.1 Formulation

The error analysis algorithm performs a linear analysis using Jacobians calculated by the operational OCO-2 forward model. This section closely follows the discussion in Connor et al, (2008).

As defined in JPL (2015),  $\mathbf{S}_a$  is the *a priori* covariance matrix,  $\mathbf{S}_e$  is the measurement error covariance matrix, and  $\mathbf{K}$  is the weighting function (Jacobian) matrix. The off-line calculations are more detailed and more realistic than error estimates performed operationally. For example, if forward model errors are included in the  $\mathbf{S}_e$  matrix used operationally, the retrieved state may be systematically biased by the *a priori* state. Thus we evaluate the effect of forward model errors off-line. Further, evaluation

of the smoothing and interference errors strictly requires the covariance of the ensemble of true states,  $\mathbf{S}_e$ , which is not necessarily equal to the *a priori* covariance  $\mathbf{S}_a$  (Rodgers & Connor, 2003). The authors' experience with other remote sensing retrievals suggests that the *a priori* constraint, embodied in  $\mathbf{S}_a$ , should be as uniform as practical over all soundings, to avoid introducing an additional source of variability. However, the covariance of true states,  $\mathbf{S}_e$ , varies with latitude, longitude, and season. Estimates of  $\mathbf{S}_e$  are readily included in the off-line error estimates. (See for example section 3.3.1.)

Equations 1 through 6 follow the definitions of Rodgers (2000) and Rodgers & Connor (2003). Given  $\mathbf{K}$ ,  $\mathbf{S}_e$ , and  $\mathbf{S}_a$ , we first characterize the operational retrieval by calculating the gain function  $\mathbf{G}_y$  and the averaging kernel matrix  $\mathbf{A}$ :

$$\mathbf{G}_y = (\mathbf{K}^T \mathbf{S}_e^{-1} \mathbf{K} + \mathbf{S}_a^{-1})^{-1} \mathbf{K}^T \mathbf{S}_e^{-1} \quad (1)$$

and

$$\mathbf{A} = \mathbf{G}_y \mathbf{K} \quad (2)$$

We then specify a list of estimated errors to include in the calculation, and where possible the correlation between errors. We will refer to these as 'error sources.' Next we assemble these into an ensemble covariance  $\mathbf{S}_e$  (for elements in the state vector) and a forward model parameter covariance  $\mathbf{S}_p$  (for elements not included in the state vector). Finally, we calculate the Jacobian matrix with respect to the forward model parameters, denoted  $\mathbf{K}_p$ .

For each error in the list, we calculate the resulting covariance of the retrieved state vector, as follows. For measurement error,

$$\hat{\mathbf{S}}_m = \mathbf{G}_y \mathbf{S}_\delta \mathbf{G}_y^T \quad (3)$$

where  $\mathbf{S}_\delta$  may be equal to  $\mathbf{S}_e$ , or an alternative estimate of the actual measurement covariance. In the work presented here,  $\mathbf{S}_\delta = \mathbf{S}_e$ .



For forward model error,

$$\hat{\mathbf{S}}_f = \mathbf{G}_y \mathbf{K}_b \mathbf{S}_b \mathbf{K}_b^T \mathbf{G}_y^T \quad (4)$$

180 For smoothing error,

$$\hat{\mathbf{S}}_s = (\mathbf{A} - \mathbf{I}) \mathbf{S}_c (\mathbf{A} - \mathbf{I})^T \quad (5)$$

where  $\mathbf{I}$  is the identity matrix.

185

And for interference error, which refers to error in  $\text{CO}_2$  caused by non- $\text{CO}_2$  components of the state vector

$$\hat{\mathbf{S}}_i = \mathbf{A}_{ue} \mathbf{S}_{ee} \mathbf{A}_{ue}^T \quad (6)$$

190

where  $\mathbf{S}_{ee}$  is the ensemble covariance for the non  $\text{CO}_2$  elements  $\mathbf{e}$ , and  $\mathbf{A}_{ue}$  is the off-diagonal block of the averaging kernel matrix which relates  $\mathbf{e}$  to the  $\text{CO}_2$  profile  $\mathbf{u}$ .

Finally, the total covariance is

195

$$\hat{\mathbf{S}} = \hat{\mathbf{S}}_m + \hat{\mathbf{S}}_s + \hat{\mathbf{S}}_i + \hat{\mathbf{S}}_f \quad (7)$$

and the resulting variance of  $X_{\text{CO}_2}$  is  $\sigma_{X_{\text{CO}_2}}^2 = \mathbf{h}^T \hat{\mathbf{S}} \mathbf{h}$ , where  $\mathbf{h} = \partial X_{\text{CO}_2} / \partial \mathbf{x}$

represents the pressure weighting function. Alternatively, one may calculate the

200

variance in  $X_{\text{CO}_2}$  due to a given error source,  $r$ , as  $\sigma_r^2 = \mathbf{h}^T \hat{\mathbf{S}}_r \mathbf{h}$  and sum the variances for all  $r$ .

The discussion of the preceding paragraph makes two assumptions. One, that the retrieval is approximately linear within the region bounded by its uncertainty, and

205

two, that the error sources considered are themselves uncorrelated. Whenever error sources are correlated, the correlations must be included in, e.g. Eq (4) or (6), and the net effect on  $X_{\text{CO}_2}$  calculated for the combined correlated sources.

## 2.2 Treatment of Fixed Error Sources

210 Many of the error sources we will consider do not vary randomly, and some do not  
vary at all. Spectroscopic errors belong to the class of error sources which are truly  
fixed. Unfortunately, due to the varying amount of information in each measured  
spectrum relative to the *a priori* constraint, embodied in changes in the gain function,  
 $\mathbf{G}_y$ , the resulting errors in retrieved  $\text{XCO}_2$  are not fixed. We will treat such errors as  
215 follows.

We note that the gain function,  $\mathbf{G}_y$ , represents the sensitivity of the state vector to the  
measured radiances. Combining that with the definition of  $\mathbf{K}_b$ , and considering for the  
moment a single scalar parameter, the error caused by parameter  $\mathbf{b}$  is

220

$$\hat{\mathbf{x}} - \mathbf{x} = \mathbf{h}^T \mathbf{G}_y \mathbf{K}_b \mathbf{d}\mathbf{b} \quad (8)$$

where  $\hat{\mathbf{x}} - \mathbf{x}$  is the retrieved  $\text{XCO}_2$  minus the true  $\text{XCO}_2$ , or we may write

225

$$\hat{\mathbf{x}} - \mathbf{x} = (\mathbf{h}^T \mathbf{G}_y \mathbf{K}_b \mathbf{d}\mathbf{b}^2 \mathbf{K}_b^T \mathbf{G}_y^T \mathbf{h})^{1/2} \quad (9)$$

Replacing  $\mathbf{d}\mathbf{b}^2$  with its matrix equivalent  $\mathbf{S}_b$ , then for an ensemble of retrievals,

$$\sigma_x = \text{rms}(\hat{\mathbf{x}} - \mathbf{x}) = \text{rms}[(\mathbf{h}^T \mathbf{G}_y \mathbf{K}_b \mathbf{S}_b \mathbf{K}_b^T \mathbf{G}_y^T \mathbf{h})^{1/2}] \quad (10)$$

230

So if  $\mathbf{d}\mathbf{b}$  is a constant, the error  $\hat{\mathbf{x}} - \mathbf{x}$  caused by it will vary about a mean value given  
by  $\sigma_x$ . While the true error in parameter  $\mathbf{b}$  is an unknown constant, we assume that  
error is equal to the uncertainty in  $\mathbf{b}$ .

235

## 2.3 Variable Error

Sources and sinks of  $\text{CO}_2$  and the circulation of the atmosphere produce temporal and  
spatial gradients in the  $\text{XCO}_2$  field, which are quantitatively predicted by carbon cycle  
models. Measuring these gradients is a strong test of such models. Thus, errors which

vary from sounding to sounding limit the efficacy of the OCO-2 measurements in  
constraining carbon cycle models. On the other hand, an error which is constant, or at  
least has a well-defined mean value, can be subtracted from all soundings with  
minimal or no effect on gradients of XCO<sub>2</sub>. Therefore, we have attempted to  
distinguish the uncertainty which differs between soundings, i.e. applies to a  
difference in two soundings, from the total accuracy.

We will refer to this differential uncertainty as ‘variable error’. By its nature, variable error has both random components and those which are systematic in the sense that they depend on conditions such as solar zenith angle, atmospheric temperature, pressure, and aerosol, and surface properties. In other words, the concept of variable error applies to the difference between any two soundings, but its magnitude will depend on the difference in conditions between them.

Our quantitative estimate of variable error is a composite error calculated from a selection taken from all error sources described above. Variable error will be calculated from all error sources, but will exclude the mean error produced by fixed error sources as discussed in Sect. 2.2. Then a first approximation to the predicted error in the difference of XCO<sub>2</sub> between two soundings will simply be the variable error multiplied by  $\sqrt{2}$ , assuming remaining errors are uncorrelated in space or time. This should be equivalent to estimating the net uncertainty in each sounding, and assuming a simple bias correction relative to validation observations has been performed.

Brian Connor 22/9/2016 9:35 AM

**Deleted:** The term ‘variable error’ will be used to refer to

### 270 3. Error Types

We will consider four types of error: measurement, smoothing, interference, and forward model.

#### 275 3.1 Measurement error

The first and most obvious error is random noise in the measured spectrum. This is calculated based on the operational noise model (JPL, 2015), and its direct effect on XCO<sub>2</sub> is calculated, and tabulated as ‘measurement error.’

280 However, it is observed that spectral residuals do not decrease with averaging as would be expected for pure random noise, but instead have a systematic structure. Because of this it was decided to derive empirical orthogonal functions (EOFs) representing this systematic structure, and to retrieve scale factors for these functions at every sounding. (See Section 3.3.2.6 of JPL, (2015)). Uncertainties in this process  
285 are to be addressed as interference error, below.

#### 3.2 Smoothing error

This represents error due to the *a priori* constraint of the state vector. As suggested by Rodgers & Connor (2003), we have separated this into two components. The first,  
290 smoothing by the true CO<sub>2</sub> profile, which we simply refer to as ‘smoothing’, is discussed here. The second component is error introduced into XCO<sub>2</sub> by the non-CO<sub>2</sub> elements of the state vector, which we call ‘interference’, discussed in the following section.

295 The error due to the true atmospheric CO<sub>2</sub> profile would be best estimated by using the covariance of the ensemble of true states,  $S_c$ . Exactly which states to include in the ensemble is not well defined. We have chosen to use the *a priori* covariance  $S_a$ , which is intended to represent the variability of CO<sub>2</sub> globally throughout the year. We will systematically overestimate the smoothing error as a result. However, the smoothing  
300 error is always small, as we will see, and the use of  $S_a$  is fundamentally conservative.

Brian Connor 22/9/2016 9:35 AM

Formatted: Font:Bold

### 3.3 Interference error

#### 3.3.1 Aerosol and Cloud

We apply the Modern Era Retrospective analysis for Research and Applications (MERRA) aerosol reanalysis climatology for daytime (local time 10:00 AM, 1:00 PM, and 4:00 PM) in June and December, to represent the aerosol related variability in the OCO-2 spectral measurements (Rienecker et al., 2011). [The MERRA aerosol data is the basis for the OCO-2 forward model's aerosol types, as described in detail in JPL, 2015, p 28-31.](#) MERRA aerosol data consisting of five composite types, namely dust (DU), sea salt (SS), sulfate (SU), black carbon (BC), and organic carbon (OC), have nearly zero bias and a correlation coefficient of  $\sim 0.9$  with respect to the collocated Aerosol Optical Depth (AOD) measurements from AErosol RObotic NETwork (AERONET), Multi-angle Imaging SpectroRadiometer (MISR), and Ozone Monitoring Instrument (OMI) (Buchard et al., 2015). At each sounding location, the two composite types most common at that location are included in the state vector for the operational retrieval, along with liquid water and ice cloud, and are retrieved by the L2 algorithm. For the analysis presented here we take into account the variability of all five type of aerosols, including those not retrieved, as described next.

The L2 calculations for linear error analysis are performed at each sounding with the operational state vector and *a priori* uncertainties, augmented as follows. Ten additional aerosol quantities are added to the state vector, namely the AOD for each of the 5 composite MERRA aerosols, integrated over two layers. Using the relative pressure scale  $\sigma$ , defined as the fraction of surface pressure, the lower layer is at  $\sigma = 0.95$  with width 0.05, while the upper layer is at  $\sigma = 0.5$  with width 0.2. The *a priori* amount and uncertainty for each of these 10 aerosol quantities is set equal to a small positive number, non-zero to avoid singularity, but small enough to have negligible effect on the algorithm. The L2 algorithm then calculates the Jacobians for each of these 10 interfering aerosol species.

Subsequently, the linear error analysis combines the Jacobians for all of the aerosol and cloud quantities (liquid water, ice, the 2 types retrieved, and the 10 additional interfering aerosols) with estimates of the ensemble variability of their total atmospheric AOD, to calculate the resulting error in XCO<sub>2</sub>. For this step, we have created a database of the standard deviation of each of the 5 MERRA composite types, in 2 layers defined as the surface to 750 hPa and 750 hPa to top of atmosphere, on a 2.5 x 2.5 degree lat/lon grid, for each month. For each sounding location, our error analysis algorithm looks up the standard deviation at the nearest grid point for all 10 aerosols, and uses that as the estimated ensemble variability. For liquid water and ice cloud, we assume the ensemble variance equals the *a priori* variance. The *a priori* uncertainty of liquid water and ice (approximately a factor 6 (1 $\sigma$ )) was deliberately set large enough to minimize its effect on retrieved XCO<sub>2</sub>.

The two retrieved aerosol types are counted twice by this procedure, once in the operational state vector and again in the part of the state vector as augmented for the error analysis. To avoid an error due to ‘double counting’, we set the ensemble variance for the aerosols in the operational state vector to very small values, ensuring they produce negligible error in retrieved XCO<sub>2</sub>.

### 3.3.2 Empirical Orthogonal Functions (EOFs)

Interference errors due to the scale factors applied to the operational EOFs are calculated as part of the error analysis by including the actual EOF scale factors in the state vector. The results show negligible effects on XCO<sub>2</sub> uncertainties and degrees of freedom due to these scale factors.

### 3.3.3 Other Interference Errors

Other non-CO<sub>2</sub> components of the state vector include surface pressure, water vapor column, an offset to the *a priori* temperature, a linear dispersion coefficient for each spectral band (defining the separation in wavelength between adjacent pixels), albedo, and the linear change in albedo across each spectral band. Land (nadir) observations also include a coefficient of fluorescence, and ocean (glint) observations include wind speed. These have all been included in the error analysis.

For all of these components, an effort has been made to include an estimate of global variability as the *a priori* uncertainty, and this has been used as the estimated ensemble variability in the error analysis. The net effect of these uncertainties is fairly small compared to aerosols and forward model errors, so refining this ensemble estimate has not been a high priority, but may be considered later.

### 3.4 Forward Model Error

Forward model errors which have been evaluated in this analysis include those due to a variety of spectroscopic and calibration parameters.

Table 1 shows the estimated uncertainties in spectroscopic parameters used in the L2 algorithm. The parameters listed are those required for the spectroscopic line shape models used within the OCO-2 v7 L2 algorithm. For CO<sub>2</sub> this is a speed-dependent Voigt line shape with tridiagonal line mixing and for O<sub>2</sub>, this is a Voigt line shape with first order line mixing, with a contribution from collision-induced absorption (CIA). The relevant references, describing these parameters and the uncertainty estimates, are given in the Table.

The majority of the uncertainties listed in Table 1 are based on published values. The notable exceptions are speed dependence in the CO<sub>2</sub> bands, and line mixing in the O<sub>2</sub> A-band. Fairly large uncertainties have been estimated for these by L. Brown at JPL (private communication 2014).

It is also worth noting that the exponent of the temperature dependence of the pressure broadened linewidths in the O<sub>2</sub>-A band has been measured recently by Droiun et al (2015). The absolute value of this parameter differs by ~8% from the previously published value (Brown & Plymate, 2000) which was used in the OCO-2 data processing up to and including v7. The newer, Drouin et al value will change the derived XCO<sub>2</sub> values by ~ 1 ppm.

Also of note is a discrepancy between recent measurements of the line strength in the WCO<sub>2</sub> band. The values used by the OCO-2 algorithm are based on Devi et al (2007, 2016). Values from Polyansky et al (2015) differ from those in Devi et al (2016) by ~1.2%.

Spectroscopic uncertainties in interfering gas species are not a significant source of error in retrieved XCO<sub>2</sub>. The strongest interferent, by far, is H<sub>2</sub>O, and its largest uncertainties are in its pressure broadening. Earlier tests of the L2 algorithm (not part of the present analysis) evaluated H<sub>2</sub>O line parameters with broadening coefficients 20% different from reference values, and found mean XCO<sub>2</sub> changes of < 0.01 ppm, with apparently random distribution. Therefore we have not included spectroscopic uncertainties in any interfering species in Table 1, and will not discuss them further.

Uncertainties in the calibration parameters are shown in Table 2. These are based on pre-flight laboratory calibration of the instrument at the Jet Propulsion Laboratory. The parameters are defined as follows. The instrument line shape (ILS) in each band is assumed to have a single uncertainty, in its width. Its shape as measured in the laboratory before launch is assumed to be correct. Radiometric gain is the factor applied to the measured voltages to convert them to absolute physical units. Finally, OCO-2 is only sensitive to one polarization of the incoming radiation, whose angle of orientation is the ‘polarization angle’.

In applying the uncertainties in polarization angle, we note that the observed spectrum **S** may be written in terms of the Stokes parameters **I**, **Q**, **U**, and **V**, and Mueller matrix coefficients **m<sub>I</sub>**, **m<sub>Q</sub>**, **m<sub>U</sub>**, and **m<sub>V</sub>**:

$$\mathbf{S} = m_I \mathbf{I} + m_Q \mathbf{Q} + m_U \mathbf{U} + m_V \mathbf{V} \quad (11)$$

Uncertainties in the Mueller matrix coefficients were calculated as follows:

First,

$$\begin{aligned} m_I &= 0.5 \\ m_Q &= 0.5 * \cos(2 * \phi_{pol}) \\ m_U &= 0.5 * \sin(2 * \phi_{pol}) \\ m_V &= 0 \end{aligned}$$



The uncertainty in the polarization angle  $\Phi_{\text{pol}}$  is  $\pm 0.5^\circ$  (Table 2,  $1\sigma$ ) for all 3 bands,  $m_Q$  and  $m_U$  are derived from the same measurement, so have correlation = 1, and the 3 bands should be independent. From the above, a 3 x 3 covariance matrix can readily be calculated which applies to all 3 bands (uncertainty in  $m_I$  is assumed to be non-zero, but very small, to avoid singularity). Note that  $V$ , the circular component of polarizat<sub>on</sub>, is completely ignored in the L2 algorithm as there are very few natural sources.

#### 4. Results

Figures 1 through 6, and Tables 3 and 4, below, display the summary of results for the off-line error analysis. The data are gridded into 10 by 10 degree bins and only bins with a minimum of 3 soundings are displayed. An overall observation is that there is some spatial seasonal dependence in all of the error types due to the shifting sub solar point of the sun from summer to winter which drives signal and air mass related errors.

Figure 1 shows measurement error, due to random noise in the measured spectra. It is typically  $\sim 0.5$  ppm for a single sounding, and is expected to decrease with averaging approximately as expected for random error, i.e. in proportion to  $\sqrt{N}$ , for  $N$  = number of soundings in the average. The error is smaller and more uniform for ocean than land, presumably due to the increased SNR in glint viewing mode.

Forward model error, divided into spectroscopic and instrument error, is shown in Figs. 2 and 3, respectively. Spectroscopic and instrument error make roughly equal contributions to forward model error. Spectroscopic error in ocean glint observations shows little variation, and is  $\sim 1.3$  ppm. For land nadir it is more variable, typically 1-2 ppm. The most important spectroscopic error is due to uncertainty in the  $WCO_2$  band strength (Tables 3, 4). Instrument error is somewhat more variable, especially over land. It is  $\sim 1$  ppm in ocean glint and  $\sim 0.5$ -2.5 in land nadir. The most important instrument error is due to uncertainty in the instrument line shape (ILS).

Maps of aerosol error are shown in Fig. 4a, and for comparison, the monthly mean aerosol optical depth from MERRA is shown in Fig 4b, and its standard deviation in Fig 4c. The sensitivity of XCO<sub>2</sub> to interference error caused by the various aerosol types is shown in the Supplementary Material published with this paper.

In most places, aerosol errors are surprisingly small, typically ~0.5 ppm. However there are regions where they are systematically larger, ~ 2.0 - 2.5 ppm. These regions include east Asia, which has highly variable aerosol loading, and the tropical North Atlantic, due to dust (not shown), presumably from North Africa. There are also systematically large errors over the Arctic Ocean. We believe these occur because of high sensitivity of the algorithm to small spectral errors at high solar zenith angle.

Variable error is shown in Fig. 5. Comparison to Figs. 3 and 4 shows that variable error over land is dominated by instrument error (due to instrument line shape), but by aerosol error over ocean. It is typically ~0.5 – 2.0 ppm in land nadir, and mostly < 1 ppm in ocean glint, but as for aerosol, it is 2.0 - 2.5 ppm in glint in some regions.

Total error from all sources is shown in Fig. 6. It is ~1.5 - 3.5 ppm over land and ~1.5 - 2.5 ppm over ocean.

## 5. Discussion

Inspection of the global mean and standard deviations in Tables 3 and 4 gives rise to some interesting observations. In general, the fixed, or approximately fixed, error sources (spectroscopy and instrument calibration), cause mean errors much larger than their standard deviations. This implies that whatever the true value of the error in the relevant forward model parameter, most of its effect can in principle be removed by simple bias correction based on validation measurements. However, the remaining, variable error, caused by the fixed error source, is of critical importance. The error in the difference in XCO<sub>2</sub> between two soundings is better characterized by the variability of that parameter's effect than by its mean; i.e the mean effect is the same for both soundings and is removed by taking their difference. This is the rationale for our definition and use of Variable Error, as discussed in Sect. 3. It is also worth noting

Brian Connor 22/9/2016 9:35 AM

Deleted:

Brian Connor 22/9/2016 9:35 AM

Deleted: .

Brian Connor 22/9/2016 9:35 AM

Deleted: main

Brian Connor 22/9/2016 9:35 AM

Deleted: Similarly

that both the mean and standard deviation of errors due to fixed sources is larger for land nadir than for ocean glint soundings.

505 As noted above, spectroscopic error varies little over the ocean, and modestly over land. The main sources of this behavior can be traced to WCO<sub>2</sub> and O<sub>2</sub> line strength, which are the largest error sources but are fairly constant in both regimes, and SCO<sub>2</sub> and O<sub>2</sub> line mixing, which have highly variable effects over land, and little variation over ocean.

510

Three components of instrument error were analyzed. Error due to uncertainty in the polarization angle  $\Phi_{\text{pol}}$  is negligible,  $< 0.01$  ppm (not shown elsewhere). Uncertainty in instrument gain is a significant but fairly small source of XCO<sub>2</sub> error, averaging 0.2-0.3 ppm. The behavior of the instrument error is dominated by the ILS;

515 uncertainties in XCO<sub>2</sub> due to the ILS are the largest single error source over land, with variability second only to aerosol ( $\sim 1.4 \pm 0.4$  ppm). Pre-flight measurements of the ILS were done to high accuracy (Table 2), but the sensitivity of XCO<sub>2</sub> to the ILS is high. Error due to the ILS is larger and much more variable over land than over ocean.

520 Uncertainty due to smoothing error is fairly small. It is typically  $\leq 0.2$  ppm. The full results (not shown) indicate it is rarely if ever larger than 0.4 ppm. The magnitude of smoothing error was deliberately minimized by choice of a loose *a priori* constraint on the CO<sub>2</sub> profile in the L2 algorithm. It is likely to vary systematically with local conditions, since it arises in the difference between the actual and *a priori* CO<sub>2</sub> profile shapes.

525

Tables 3 and 4 also emphasize that the dominant variable error is due to aerosol.

Although the absolute size of the aerosol error is fairly small, it varies widely from place to place, with a standard deviation up to 195% of its mean value (the coefficient of variations are 134%, 109%, 195%, and 132% for June nadir-land, Dec nadir-land, June glint-water and Dec glint-water, respectively). Furthermore, it will depend on the actual atmospheric aerosol distribution, which will vary in a complex fashion with space and time. Correlation of the aerosol distribution is likely to be a major source of correlation in XCO<sub>2</sub> error, which will be difficult to characterize quantitatively.

530

We envisage a continual ongoing analysis to quantify uncertainties in the OCO-2 measurements. We believe such quantification is critical for using the data to constrain the geophysical carbon cycle. Linear error analysis as presented here will be a key part of that effort, and it is important to replicate the analysis when future versions of the L2 algorithm are released and mission data are re-processed. The error analysis should be extended to further examine errors produced by the algorithm itself. This would include studying the effect of errors in algorithm inputs such as the *a priori* state vector. A more general subject for study is non-linearity of the forward and inverse models. Both of these areas are foci of active research. In the particular case of nonlinearity, linear error analysis can be supplemented with Monte Carlo studies. The Monte Carlo approach can interrogate the probability distribution of retrieval errors under specified conditions and can characterize correlations between multiple error sources, such as interference and nonlinearity, for example. Monte Carlo studies require far more computational effort than the linear error analysis, so experiments should be designed for a carefully selected subset of conditions.

Specific recommendations for linear error analysis include the following. Linear error analysis, as applied here to simulations, will be used to estimate uncertainties in selected sets of actual OCO-2 measurements. This work will have two main goals. First, we will analyze sets of OCO-2 measurements which have been used for ‘top-down’ error estimates and validation, by comparison to TCCON data and by examining observed scatter in uniform, local areas. The volume of OCO-2 data has provided a large collection of validation datasets for many regions, spanning all seasons. The results of these ‘top-down’ estimates will be compared to the ‘bottom-up’ estimates of linear error analysis. If these two types of estimates are consistent they will give us confidence in our overall understanding of measurement uncertainty. Any inconsistencies will require further investigation. One possible source of inconsistencies, already under investigation as described above, is non-linearity of the forward model.

Second, the variability of the bottom-up estimates will be systematically compared to the variation in sounding geometry, atmospheric conditions, and surface type. This

will improve insight into the causes of measurement uncertainty, and guide data users in quantitative applications.

#### Acknowledgements:

We thank the following members of the OCO-2 team for support and helpful discussions: Vijay Natraj, Linda Brown, Brian Drouin, Chris Benner, Malathy Devi, and Annmarie Eldering. Part of the research was carried out at the Jet Propulsion Laboratory, California Institute of Technology, under a contract with the National Aeronautics and Space Administration. The CSU contribution to this work was supported by JPL subcontract 1439002. The contribution by BC Scientific Consulting was supported by JPL subcontract 1518224.

#### References:

Benner D.C., Devi V.M., Nugent E., Sung K., Brown L.R., Miller C.E. et al. (2011), Line parameters of carbon dioxide in the 4850 cm<sup>-1</sup> region. *Twenty-second Coll. on High Res. Mol. Spectrosc.*, Dijon, France, 2011; poster N19.

[Boesch, H., D. Baker, B. Connor, D. Crisp and C. Miller, \(2011\). Global Characterization of CO<sub>2</sub> Column Retrievals from Shortwave-Infrared Satellite Observations of the Orbiting Carbon Observatory-2 Mission, \*Remote Sens.\*, 3\(2\), 270-304.](#)

Buchard V., da Silva A. M., Colarco P. R., Darmenov A., Randles C. A., Govindaraju R., Torres O., Campbell J., and Spurr R. (2015). Using the OMI aerosol index and absorption aerosol optical depth to evaluate the NASA MERRA Aerosol Reanalysis, *Atmos. Chem. Phys.*, 15, 5743-5760.

[Butz A., Hasekamp, O.P., Frankenberg, C., Aben, I. \(2009\). Retrievals of atmospheric CO<sub>2</sub> from simulated space-borne measurements of backscattered near-infrared sunlight: accounting for aerosol effects, \*Appl. Opt.\* 48, No. 18.](#)

Connor, B. J., Bösch, H., Toon, G., Sen, B., Miller, C., and Crisp, D. (2008), Orbiting Carbon Observatory: Inverse method and prospective error analysis, *J. Geophys. Res.*, 113, D05305, doi:10.1029/2006JD008336.

Crisp, D., Miller, C., and DeCola, P. (2008), NASA Orbiting Carbon Observatory; measuring the columnaveraged carbon dioxide mole fraction from space, *J. Appl. Remote Sens.*, 2, 023508, doi:10.1117/1.2898457.

Brian Connor 22/9/2016 9:35 AM  
Formatted: Indent: Left: 0 cm

- 615 Devi, V. M., Benner, D.C., Brown, L.R., Miller, C.E., and Toth, R.A. (2007), Line mixing and speed dependence in CO<sub>2</sub> at 6227.9 cm<sup>-1</sup>: Constrained multispectrum analysis of intensities and line shapes in the 30013 ← 00001 band, *J. Mol. Spectrosc.* 245, 52-80.
- 620 Devi, V.M., Benner, D.C., Sung, K., Brown, L.R., Crawford, T.J., Miller, C.E., Drouin, B.J., Payne, V.H., Yu, S., Smith, M.A.H., Mantz, A.M., and Gamache, R.R. (2016), Line parameters including temperature dependences of self- and air-broadened line shapes of <sup>12</sup>C<sup>16</sup>O<sub>2</sub>: 1.6-μm region, *J. of Quant. Spectrosc. and Rad. Transfer*, vol. 177, 117-144.
- 625 Drouin, B.J., Benner, D.C., Brown, L.R., Cich, M.J., Crawford, T.J., Devi, V.M., Guillaume, A., Hodges, J.T., Mlawer, E.J., Robichaud, D.J., Oyafuso, F., Payne, V.H., Sung, K., Wishnow, E.H., and Yu, S. (2016). Multispectrum analysis of the oxygen A-band, *J. of Quant. Spectrosc. and Rad. Transfer*, in press.
- 630 Joly, L., Marnas, F., Gibert, F., Bruneau, D., Grouiz, B., Flamant, P.H., Durry, G., Dumelie, N., Parvitte, B., and Zeninari, V., (2009). Laser diode absorption spectroscopy for accurate CO<sub>2</sub> line parameters at 2 microns: consequences for space-based DIAL measurements and potential biases, *Applied Optics*, vol. 48 (29), 5475-5483
- 635 JPL, OCO-2 Level 2 Full Physics Retrieval Algorithm Theoretical Basis, Version 2.0 Rev 2, March 13, 2015: [http://disc.sci.gsfc.nasa.gov/OCO-2/documentation/oco-2-v6/OCO2\\_L2\\_ATBD.V6.pdf](http://disc.sci.gsfc.nasa.gov/OCO-2/documentation/oco-2-v6/OCO2_L2_ATBD.V6.pdf)
- 640 [Jung, Y., Kim, J., Kim, W. Boesch, H., Lee, H., Cho, C. Tae-Young, G. \(2016\). Impact of Aerosol Property on the Accuracy of a CO<sub>2</sub> Retrieval Algorithm from Satellite Remote Sensing, \*Remote Sens.\* 8\(4\), 322. doi:10.3390/rs8040322](#)
- 645 Lee, R.A.M., O'Dell, C.W., Wunch, D., Roehl, C.M., Osterman, G.B., Blavier, J.-F., Rosenberg, R., Chapsky, L., Frankenberg, C., Hunyadi-Lay, S.L., Fisher, B.M., Rider, D.M., Crisp, D., and Pollock, R. (2016). Preflight Spectral Calibration of the Orbiting Carbon Observatory, *IEEE Trans. on Geoscience and Remote Sensing*, submitted.
- 650 Long, D.A., Robichaud, D.J., and Hodges, J.T., (2012). Frequency-stabilized cavity ring-down spectroscopy measurements of line mixing and collision-induced absorption in the O<sub>2</sub> A-band, *J. Chem. Phys.* 137, 014307; doi: 10.1063/1.4731290
- 655 Long, D.A., Havey, D.K., Okumura, M., Miller, C.E., and Hodges, J.T., (2010). O<sub>2</sub> A-band line parameters to support atmospheric remote sensing, *J. of Quant. Spectrosc. and Rad. Transfer*, 111, 14, 2021-2036, ISSN 0022-4073, 10.1016/j.jqsrt.2010.05.011.
- O'Brien, D. M., Polonsky, I., O'Dell, C., and Carheden, A. (2009), Orbiting Carbon

- 660 Observatory (OCO), Algorithm Theoretical Basis Document, the OCO  
simulator, *Technical Report* ISSN 0737-5352-85, Cooperative Institute for  
Research in the Atmosphere, Colorado State University, Fort Collins, CO,  
USA.
- 665 O'Dell, C.W., Connor, B., Bösch, H., O'Brien, D., Frankenberg, C., Castano, R.,  
Christi, M., Eldering, A., Fisher, B., Gunson, M., McDuffie, J., Miller, C.,  
Natraj, V., Oyafuso, F., Polonsky, I., Smyth, M., Taylor, T., Toon, G.,  
Wennberg, P., and Wunch, D., (2012). The ACOS CO<sub>2</sub> retrieval algorithm –  
Part 1: Description and validation against synthetic observations. *Atmos.*  
670 *Meas. Tech.*, 5, 99-121.
- Polyansky, O.L., Bielska, K., Ghyssels, M., Lodi, L., Zobov, N.F., Hodges, J.T., and  
Tennyson, J., (2015), High-accuracy CO<sub>2</sub> line intensities determined from  
theory and experiment, *Phys. Rev. Lett.* 114, 243001,  
675 doi:10.1103/PhysRevLett.114.243001.
- Rienecker M.M., Suarez M.J., Gelaro R., Todling R., Bacmeister J., Liu E.,  
Bosilovich M.G., Schubert S.D., Takacs L., Kim G.-K., Bloom S., Chen J.,  
Collins D., Conaty A., da Silva A., Gu W., Joiner J., Koster R.D., Lucchesi R.,  
680 Molod A., Owens T., Pawson S., Pegion P., Redder C.R., Reichle R.,  
Robertson F.R., Ruddick A.G., Sienkiewicz M., and Woollen J. (2011),  
MERRA: NASA's Modern-Era Retrospective Analysis for Research and  
Applications. *J. Climate*, 24, 3624–3648.
- 685 Robichaud, D. J., Hodges, J. T., Brown, L. R., Lisak, D., Maslowski, P., Yeung, L. Y.,  
et al, (2008). Experimental intensity and line shape parameters of the oxygen  
A-band using frequency-stabilized cavity ring-down spectroscopy. *J Mol*  
*Spectrosc.*, 248, 1–13.
- 690 Rodgers C.D., (2000), *Inverse Methods for Atmospheric Sounding*, World Scientific,  
Singapore.
- Rodgers, C.D. and Connor, B.J., (2003), Intercomparison of remote sounding  
instruments. *J. Geophys. Res.* 108, D3, 4116, doi: 10.1029/2002JD002299.
- 695 Rosenberg, R., Maxwell, S., Johnson B. C., Chapsky, L., Lee R. A. M., and Pollock,  
R. (2016). Preflight Radiometric Calibration of Orbiting Carbon Observatory  
2, *IEEE Trans. on Geoscience and Remote Sensing*, in press.
- Sung, K., Brown, L.R., Toth, R.A., Crawford, T.J., (2009). Fourier transform infrared  
700 spectroscopy measurements of H<sub>2</sub>O-broadened half-widths of CO<sub>2</sub> at 4.3  $\mu$ m.  
*Can. J. of Phys.*, 87, 5, 469.
- | Taylor, T.E., O'Dell, C., Frankenberg, C., Partain, P., Cronk, H., Savtchenko, A.,  
Nelson, R., Rosenthal, E., Chang, A., Fisher, B., Osterman, G., Pollock, R.,  
Crisp, D., Eldering, A., and Gunson, M. (2016), Orbiting Carbon Observatory-  
2 (OCO-2) cloud screening algorithms; validation against collocated MODIS  
705 and CALIOP data, *Atmos. Meas. Tech.* 9, 973-989, doi:10.5194/amt-9-973-  
2016.

Brian Connor 22/9/2016 9:35 AM  
Formatted: Line spacing: single

Wunch, D., Wennberg, P., Toon, G., Connor, B., Fisher, B., Osterman, G.,  
Frankenberg, C., Mandrake, L., O'Dell, C., Ahonen, P., Biraud, S., Castano,  
710 R., Cressie, N., Crisp, D., Deutscher, N., Eldering, A., Fisher, M., Griffith, D.,  
Gunson, M., Heikkinen, P., Keppel-Aleks, G., Kyrö, E., Lindenmaier, R.,  
Macatangay, R., Mendonca, J., Messerschmidt, J., Miller, C., Morino, I.,  
Notholt, J., Oyafuso, F., Rettinger, M., Robinson, J., Roehl, C., Salawitch, R.,  
Sherlock, V., Strong, K., Sussmann, R., Tanaka, T., Thompson, D., Uchino,  
715 O., Warneke, T., and Wofsy, S., (2011), A method for evaluating bias in  
global measurements of CO<sub>2</sub> total columns from space. *Atmos. Chem. Phys.*,  
11, 12317-12337, doi:10.5194/acp-11-12317-2011.

720 Yoshida, Y. Ota, Y., Eguchi, N., Kikuchi, N., Nobuta K., Tran,, H., Morino, I.,  
Yokota, T. (2011). Retrieval algorithm for CO<sub>2</sub> and CH<sub>4</sub> column abundances  
from short-wavelength infrared spectral observations by the Greenhouse gases  
observing satellite, *Atmos. Meas. Tech.*, 4, 717–734.

Brian Connor 22/9/2016 9:35 AM

Deleted: -

... [3]

Brian Connor 22/9/2016 9:35 AM

Formatted: Indent: Left: 0 cm, First line:  
0 cm



Table 1: Uncertainties in Spectroscopic Parameters Used in the L2 Algorithm

	Band	Uncertainty	Reference
760	Line Strength		
	SCO <sub>2</sub>	0.40%	Joly et al, 2009
	WCO <sub>2</sub>	0.30%	Devi et al 2007, 2016
765	O <sub>2</sub> - A	0.40%	Long et al, 2010
	Air Broaden.		
	SCO <sub>2</sub>	0.15%	Joly et al, 2009
	WCO <sub>2</sub>	0.10%	Devi et al 2007
	O <sub>2</sub> - A	0.20%	Robichaud et al 2008
770	T – Width		
	SCO <sub>2</sub>	0.45%	Joly et al, 2009
	WCO <sub>2</sub>	0.60%	Devi et al, 2007
	O <sub>2</sub> – A	1.25%	Drouin, et al., 2016
	CIA		
775	O <sub>2</sub> – A	0.1*	Long et al, 2012
	H2O Broaden.		
	SCO <sub>2</sub>	3%	Sung et al, 2009**
	WCO <sub>2</sub>	3%	Sung et al, 2009**
	Pressure Shift		
780	SCO <sub>2</sub>	2.6%	Joly et al, 2009
	WCO <sub>2</sub>	1.5%	Devi et al 2007
	O <sub>2</sub> - A	2%	Robichaud et al 2008
	Line Mixing		
785	SCO <sub>2</sub>	10%	Benner et al, 2011
	WCO <sub>2</sub>	10%	Benner et al, 2011
	O <sub>2</sub> – A	10%	estimate**
	Speed Dep		
	SCO <sub>2</sub>	10%	estimate**
790	WCO <sub>2</sub>	10%	estimate**

\*  $10^{-7} \text{ cm}^{-1} \text{ amagat}^{-2}$

\*\* L. Brown private communication, 2014

795

800

Table 2: Uncertainties in Calibration Parameters Used in the L2 Algorithm

	Uncertainties		Correlations
805	ILS		
	O <sub>2</sub> - A	0.25%	0.7 to SCO <sub>2</sub> and WCO <sub>2</sub>
	WCO <sub>2</sub>	0.25%	0.8 to SCO <sub>2</sub>
	SCO <sub>2</sub>	0.40%	
810	Radiometric Gain		
	O <sub>2</sub> - A	1.1%	0.5 to WCO <sub>2</sub> and SCO <sub>2</sub>
	WCO <sub>2</sub>	1.5%	
	SCO <sub>2</sub>	1.6%	
815	Polarization Angle		
	O <sub>2</sub> - A	0.5°	
	WCO <sub>2</sub>	0.5°	
	SCO <sub>2</sub>	0.5°	

820

825

830

835

840

845

850

Table 3:  
Global Mean Errors in XCO<sub>2</sub> and Standard Deviations for Land Nadir Observations.  
Also shown is the coefficient of variation (relative standard deviation)

		June		December	
	Measurement	0.55 ± 0.12	22%	0.58 ± 0.12	21%
860	SCO <sub>2</sub> Line Strength	0.23 ± 0.15	65%	0.28 ± 0.18	64%
	WCO <sub>2</sub> Line Strength	0.94 ± 0.16	17%	0.92 ± 0.21	23%
	O <sub>2</sub> Line Strength	0.55 ± 0.14	25%	0.57 ± 0.09	16%
	O <sub>2</sub> Line Width	0.27 ± 0.08	30%	0.28 ± 0.05	18%
	O <sub>2</sub> Width T Dep.	0.11 ± 0.06	55%	0.19 ± 0.09	47%
865	Line Mixing SCO <sub>2</sub>	0.40 ± 0.26	65%	0.52 ± 0.36	69%
	Line Mixing O <sub>2</sub>	0.21 ± 0.17	81%	0.22 ± 0.17	77%
	Speed Dep. WCO <sub>2</sub>	0.32 ± 0.06	19%	0.34 ± 0.10	29%
	Total Spectroscopy	1.35 ± 0.17	13%	1.43 ± 0.27	19%
870	Radiometric Gain	0.15 ± 0.09	60%	0.16 ± 0.09	56%
	ILS	1.39 ± 0.44	32%	1.32 ± 0.32	24%
	Total Instrument	1.40 ± 0.43	31%	1.33 ± 0.32	24%
	Smoothing	0.15 ± 0.02	13%	0.19 ± 0.04	21%
875	Aerosol Interference	0.47 ± 0.63	134%	0.43 ± 0.47	109%
	Interference w/o aerosol	0.18 ± 0.11	61%	0.28 ± 0.16	57%
	Variable	0.93 ± 0.59	63%	0.94 ± 0.44	47%
	Total	2.16 ± 0.56	26%	2.17 ± 0.42	19%

Table 4:  
Global Mean Errors in XCO<sub>2</sub> and Standard Deviations for Ocean Glint Observations  
Also shown is the coefficient of variation (relative standard deviation)

		June		December	
	Measurement	0.35 ± 0.10	29%	0.41 ± 0.07	17%
910	SCO <sub>2</sub> Line Strength	0.27 ± 0.09	33%	0.20 ± 0.10	50%
	WCO <sub>2</sub> Line Strength	0.86 ± 0.07	8%	0.91 ± 0.09	10%
	O <sub>2</sub> Line Strength	0.74 ± 0.05	7%	0.72 ± 0.03	4%
	O <sub>2</sub> Line Width	0.37 ± 0.03	8%	0.36 ± 0.02	6%
	O <sub>2</sub> Width T Dep.	0.16 ± 0.03	19%	0.22 ± 0.08	36%
915	Line Mixing SCO <sub>2</sub>	0.07 ± 0.05	71%	0.10 ± 0.05	50%
	Line Mixing O <sub>2</sub>	0.28 ± 0.09	32%	0.23 ± 0.08	35%
	Speed Dep. WCO <sub>2</sub>	0.31 ± 0.03	10%	0.33 ± 0.03	9%
	Total Spectroscopy	1.32 ± 0.04	3%	1.35 ± 0.05	4%
920	Radiometric Gain	0.28 ± 0.10	36%	0.27 ± 0.07	26%
	ILS	0.88 ± 0.12	14%	0.84 ± 0.16	19%
	Total Instrument	0.93 ± 0.13	14%	0.88 ± 0.15	17%
	Smoothing	0.15 ± 0.02	13%	0.15 ± 0.02	13%
925	Aerosol	0.37 ± 0.72*	195%	0.19 ± 0.25	132%
	Interference w/o aerosol	0.06 ± 0.06	100%	0.08 ± 0.05	63%
	Variable	0.62 ± 0.67*	108%	0.52 ± 0.23	44%
	Total	1.77 ± 0.54*	31%	1.69 ± 0.18	11%

\*driven by Sahara dust and high latitude outliers

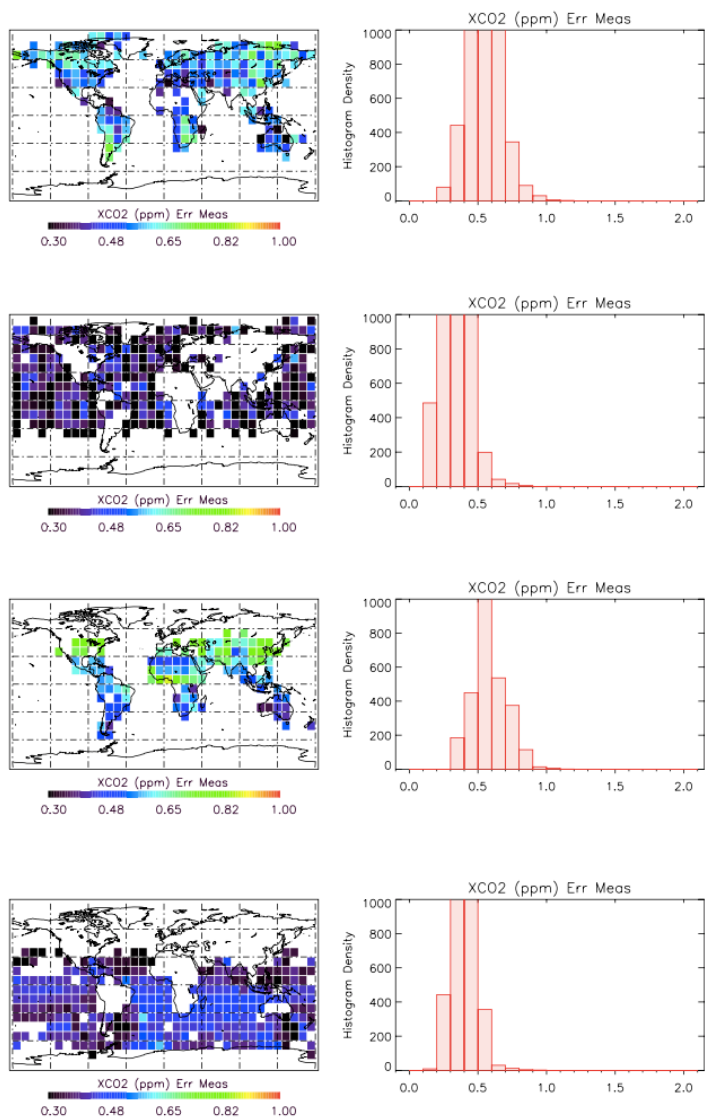


Figure 1 – Measurement Error.

Top: June, land; second: June, ocean; third: Dec. land; bottom: Dec. ocean

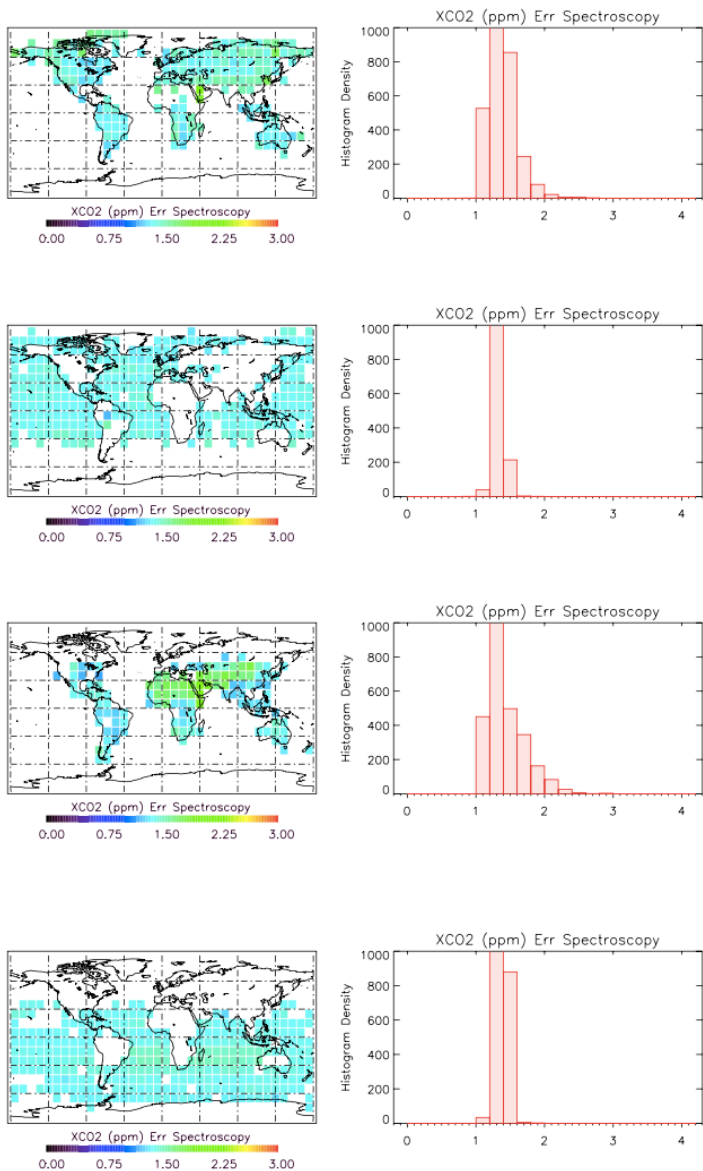


Figure 2 – Error due to spectroscopy

Top: June, land; second: June, ocean; third: Dec. land; bottom: Dec. ocean

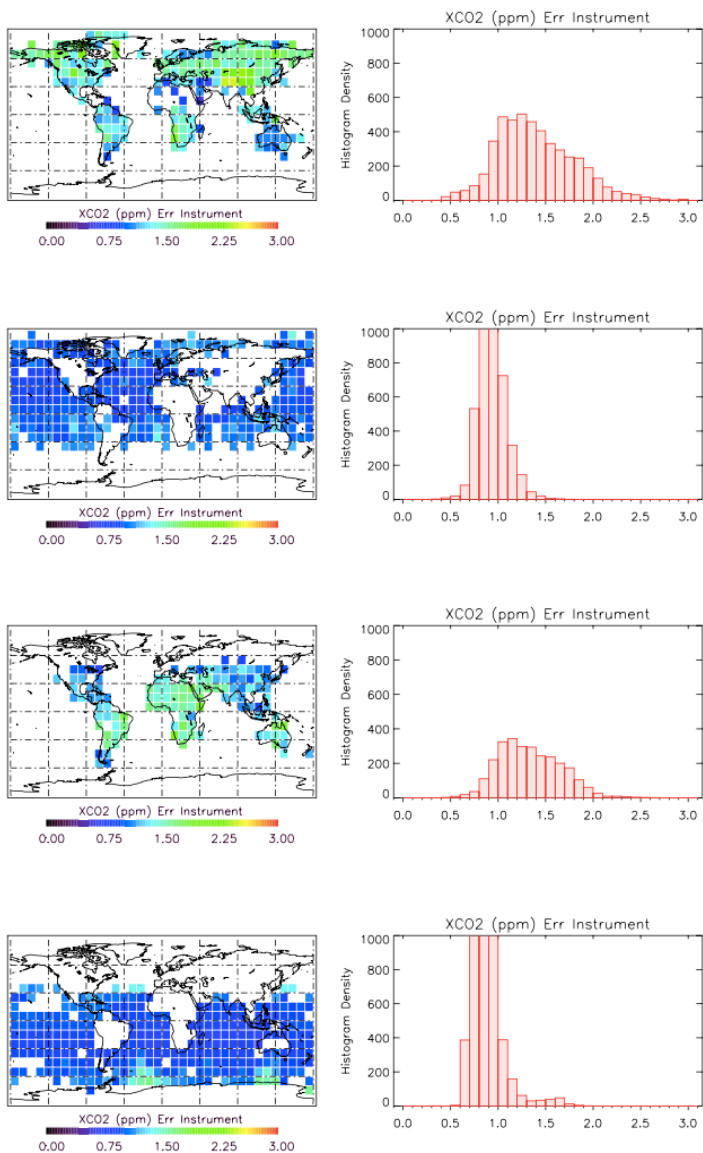
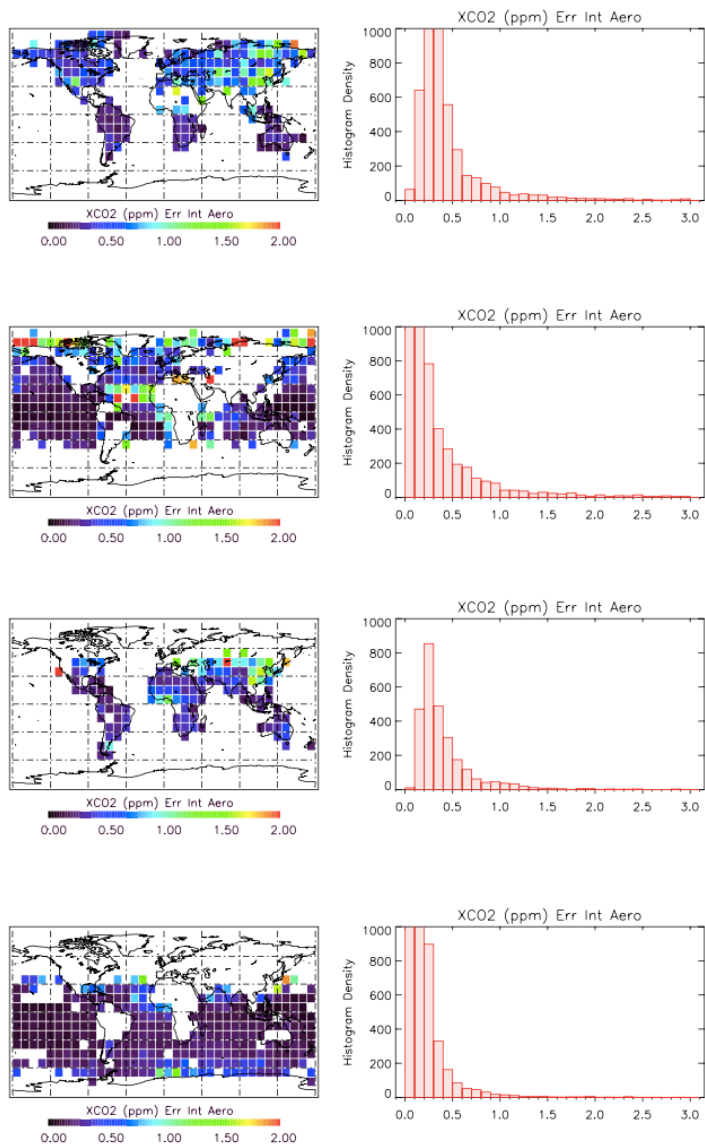


Figure 3 – Instrument Error

Top: June, land; second: June, ocean; third: Dec. land; bottom: Dec. ocean

995



1000

Figure 4a – Aerosol error

1005

Top: June, land; second: June, ocean; third: Dec. land; bottom: Dec. ocean

1010



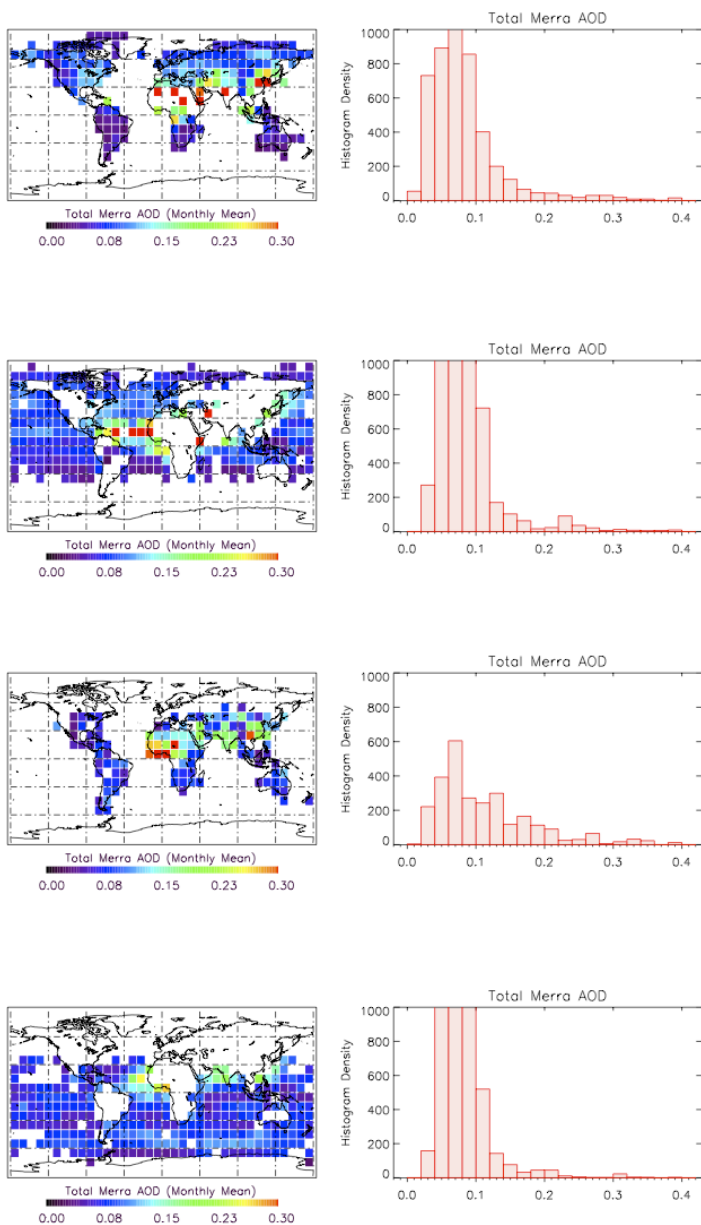


Figure 4b – Monthly Mean Aerosol Optical Depth (AOD) from MERRA

Top: June, land; second: June, ocean; third: Dec. land; bottom: Dec. ocean

Brian Connor 22/9/2016 9:35 AM  
Formatted: Indent: First line: 1.27 cm

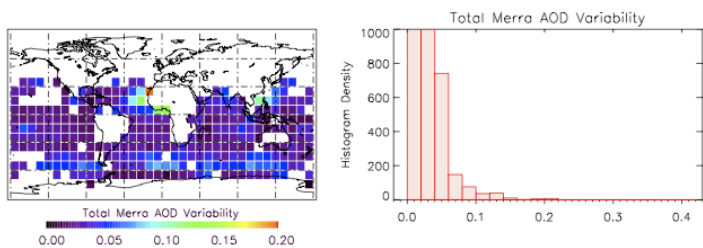
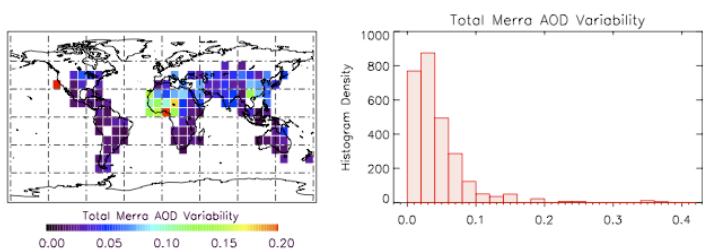
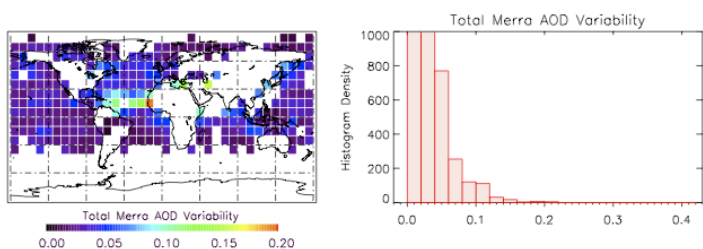
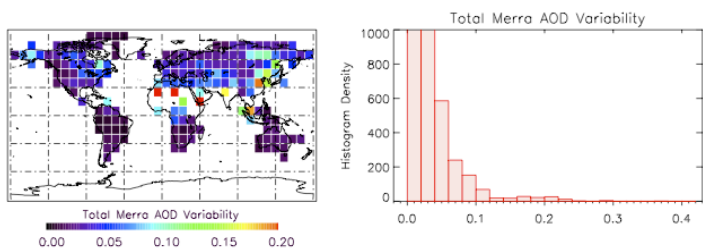


Figure 4c – Monthly Standard Deviation of Aerosol Optical Depth (AOD) from MERRA

Top: June, land; second: June, ocean; third: Dec. land; bottom: Dec. ocean

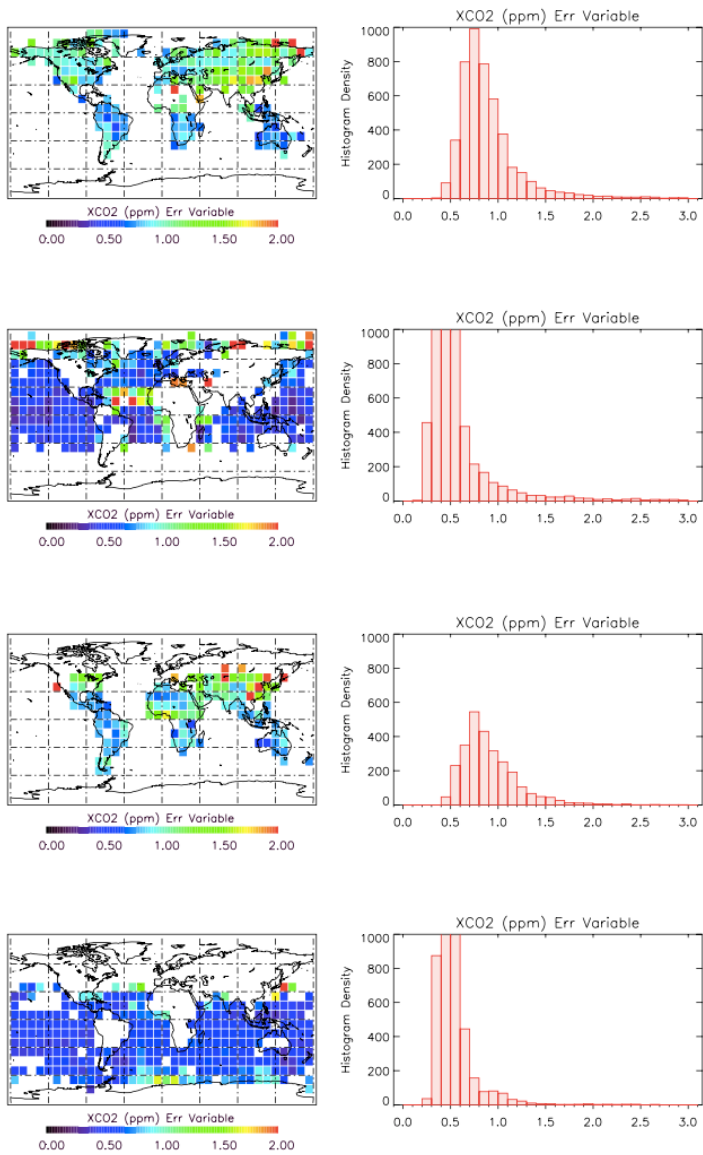


Figure 5 – Variable error

Top: June, land; second: June, ocean; third: Dec. land; bottom: Dec. ocean

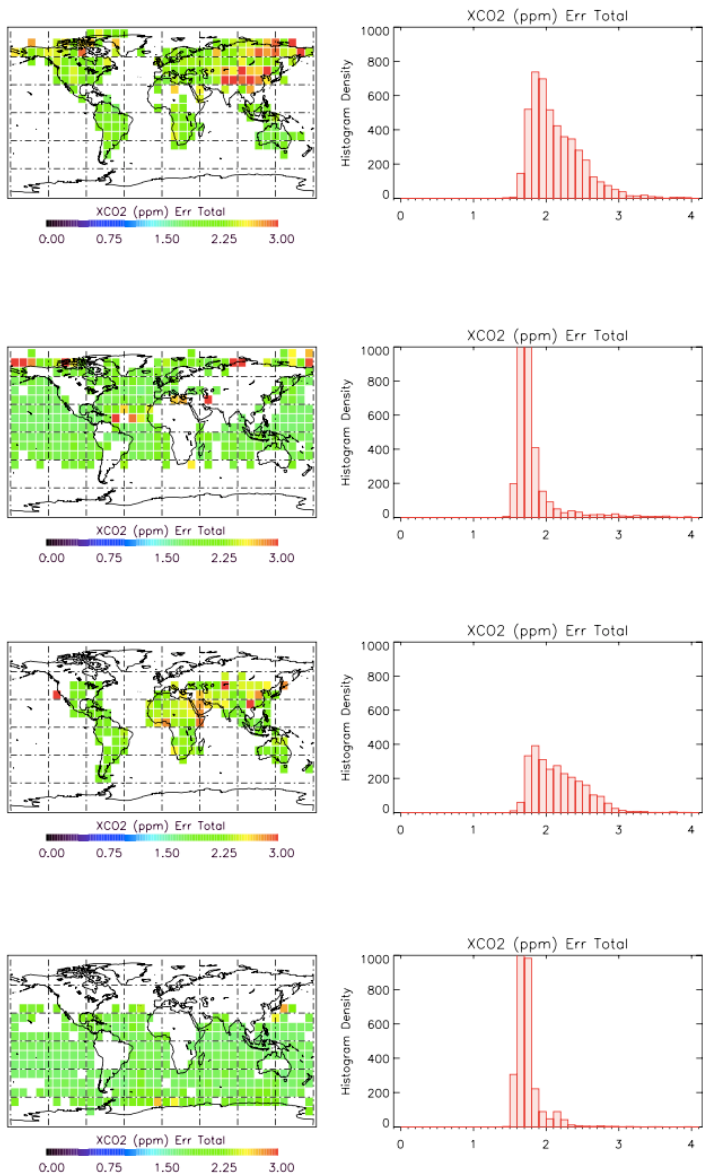


Figure 6 – Total error

Top: June, land; second: June, ocean; third: Dec. land; bottom: Dec. ocean